Gastroenterology 2025;168:53–67

Unveiling Cancer-Related Metaplastic Cells in Both *Helicobacter pylori* Infection and Autoimmune Gastritis

Stella G. Hoft,[1] Michelle Brennan,[2] Javier A. Carrero,[1] Nicholas M. Jackson,[1] Challen A. Pretorius,[1] Tarin M. Bigley,[3] José B. Sáenz,[4] and Richard J. DiPaolo[1]

[1]*Department of Molecular Microbiology and Immunology, Saint Louis University School of Medicine, St. Louis, Missouri;* [2]*Department of Biochemistry and Molecular Biology, Saint Louis University School of Medicine, St. Louis, Missouri;* [3]*Department of Pediatrics, Division of Rheumatology/Immunology, Washington University in St. Louis School of Medicine, St. Louis, Missouri; and* [4]*Division of Gastroenterology, Departments of Medicine and Molecular Cell Biology, Washington University in St. Louis School of Medicine, St. Louis, Missouri*

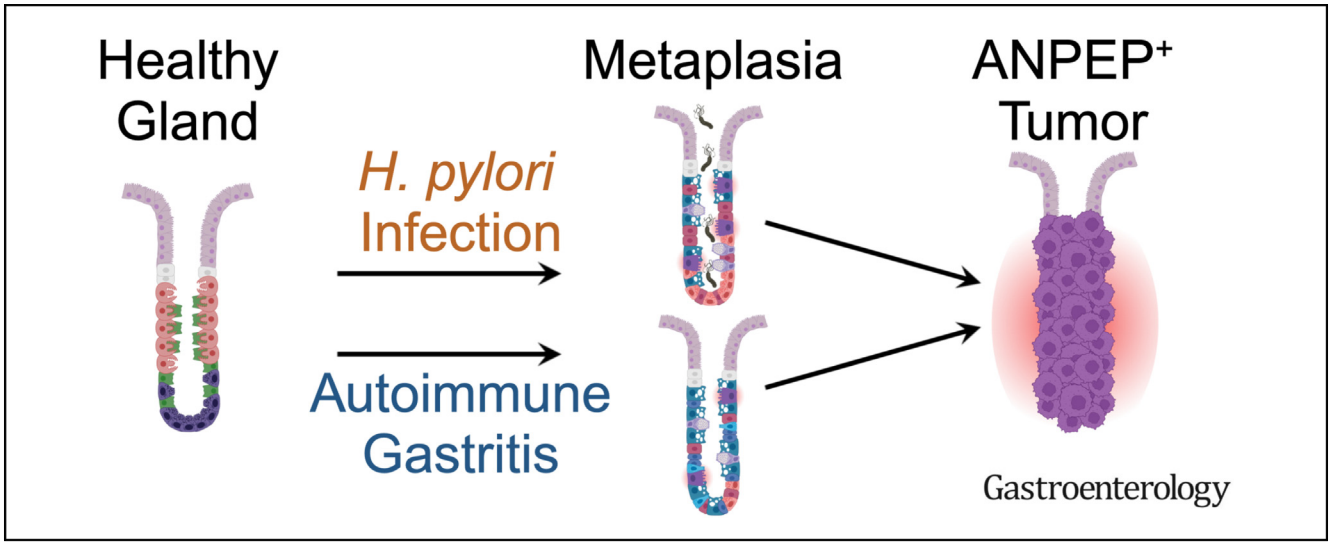

BACKGROUND & AIMS: Gastric metaplasia may arise as a consequence of chronic inflammation and is associated with an increased risk of gastric cancer development. Although *Helicobacter pylori* (*Hp*) infection and autoimmune gastritis (AIG) both induce gastric metaplasia, possible distinctions in resulting metaplastic cells and their respective cancer risks requires further investigation. **METHODS:** Using both mouse models and human participants, we scrutinized the metaplasia originating from *Hp* infection and AIG. Gastric pathology and metaplasia were examined through histopathologic assessment. Molecular features of metaplastic cells were defined using single-cell transcriptomics in murine models of *Hp* infection and AIG, as well as in human biopsy specimens from patients with *Hp* infection and AIG. Expression of a newly defined cancer-related metaplastic biomarker was confirmed through immunofluorescence. **RESULTS:** Metaplasia in *Hp* infection and AIG displayed comparable histopathologic and transcriptional features. Diverse metaplastic subtypes were identified across both disease settings, with subtle differences in the prevalence of certain subtypes between inflammatory contexts. Notably, *Hp* infection did not drive a unique metaplastic cell phenotype. One metaplastic subtype, which resembled incomplete intestinal metaplasia and shared transcriptional features with gastric cancer, was identified in both diseases. This cancer-like metaplastic subtype was characterized by expression of the cancer-associated biomarker ANPEP/CD13. **CONCLUSION:** Both *Hp* infection and AIG trigger a diverse array of metaplastic cell types. Identification of a cancer-related metaplastic cell uniquely expressing ANPEP/CD13, present in both *Hp*- and AIG-induced gastritis, indicates the carcinogenic capacity of both diseases. This discovery can guide early detection and risk stratification for patients with chronic gastritis.

Keywords: Autoimmune Gastritis; *Helicobacter pylori* Infection; Gastric Metaplasia; Gastric Cancer; Gastric Inflammation.

Gastric cancer is the fourth leading cause of cancer-related mortality, with a low 5-year survival rate due to delayed diagnosis.[1,2] Gastric metaplasia, including

Abbreviations used in this paper: **AIG, autoimmune gastritis; ANPEP, alanyl aminopeptidase N; CD, cluster of differentiation; ECL, enterochromaffin-like; GIF, gastric intrinsic factor; GKN3, gastrokine 3; *Hp*, *Helicobacter pylori*; IM, intestinal metaplasia; MHC, major histocompatibility complex; MUC6, mucin 6; SPEM, spasmolytic polypeptide expressing metaplasia; *TACSTD2*, tumor-associated calcium signal transducer 2; Tff2, trefoil factor 2; UMAP, Uniform Manifold Approximation and Projection.**

Most current article

0016-5085/$36.00
https://doi.org/10.1053/j.gastro.2024.08.032

WHAT YOU NEED TO KNOW

BACKGROUND AND CONTEXT

Gastric metaplasia increases the risk of gastric cancer. Whether *Helicobacter pylori* infection or autoimmune gastritis induce distinct metaplastic cell types with differential cancer risks is unclear.

NEW FINDINGS

Helicobacter pylori infection and autoimmune gastritis induced several subtypes of gastric metaplasia, but none were unique to *Helicobacter pylori*. Additionally, a cancer-associated metaplastic subtype was identified in patients with either *Helicobacter pylori* infection or autoimmune gastritis.

LIMITATIONS

Prospective studies, increased sample size, and advanced disease stage models will need to be used in the future to determine the cancer progression risk associated with each type of metaplasia.

CLINICAL RESEARCH RELEVANCE

Helicobacter pylori infection and autoimmune gastritis both induce a variety of metaplastic cells, some of which express cancer-related markers and may predispose to cancer. The biomarker ANPEP/CD13 can specifically identify cancer-associated, incomplete intestinal metaplasia and may be useful in improving early detection strategies during precancerous patient screenings.

BASIC RESEARCH RELEVANCE

Gastric metaplasia is histologically and transcriptionally indistinguishable in these mouse models of chronic *Helicobacter pylori* infection and autoimmune gastritis. Gastric metaplasia, in mouse models and in humans, consists of transcriptionally diverse subtypes of cells, many of which are shared between chronic *Helicobacter pylori* infection and autoimmune gastritis.

pyloric (or pseudopyloric) and intestinal types, increases the risk of gastric adenocarcinoma, with up to 90% of cancer cases arising within a field of metaplasia.[3,4] In response to acute injury, metaplasia can be reparative, resolving with resolution of the injury source.[5] However, in unresolved injury settings such as chronic inflammation, metaplasia may progress to cancer.[6] Unfortunately, methods for identifying patients at increased oncogenic risk are incompletely defined. This study was conducted to enhance our understanding of metaplasia development in the context of 2 settings of chronic inflammation: *Helicobacter pylori (Hp)* infection and autoimmune gastritis (AIG).

Different types of gastric metaplasia develop as a consequence of inflammation. Pyloric metaplasia is characterized by the appearance of pyloric region glands in the gastric corpus.[7] The base of pyloric metaplastic glands contain spasmolytic polypeptide expressing metaplasia (SPEM).[4,7] Intestinal metaplasia (IM) describes another type where gastric glands resemble the intestinal epithelium. IM can be further categorized into complete IM, where glands resemble well-differentiated small intestinal cells, and incomplete IM, where glands display both immature colonic and SPEM features.[8,9] Incomplete IM is reported to pose a higher cancer risk over complete IM and SPEM.[10] Further molecular investigation of gastric metaplasia holds the potential to facilitate earlier recognition of precancerous lesions and improve patient outcomes.

Hp infection is recognized as the primary global risk factor for gastric cancer; however, the incidence of infection has been decreasing in the United States for decades.[11,12] This juxtaposes the reported rising gastric cancer incidence among women aged <50 years, a demographic with a high incidence of autoimmunity.[13] AIG induces chronic gastritis and metaplasia, like *Hp*, and has an established association with neuroendocrine tumors, but there are conflicting reports about whether AIG increases adenocarcinoma risk as much as *Hp*.[14,15] Our study was conducted to address this topic by directly comparing the metaplasia derived from *Hp* infection and AIG in murine models and human disease.

In this study, we performed histologic and transcriptional analyses across distinct mouse models of *Hp* and AIG. By histopathology, metaplasia is strikingly similar between models. Leveraging single-cell transcriptomics, we observed transcriptional diversity among metaplastic cells in both inflammatory etiologies. To ascertain the clinical relevance of these observations, we scrutinized metaplastic cells within biopsy specimens obtained from *Hp*-infected and AIG patients. Our human investigations validated the presence of diverse metaplastic subtypes and that no unique subtypes emerged in *Hp*. Notably, we identified 1 metaplastic subtype, present in both populations, resembling incomplete IM. Transcriptionally this subtype most closely resembled gastric cancer and exhibited elevated expression of *ANPEP/CD13*, previously identified in metaplastic and cancerous gastric tissues.[16–19] Importantly, we corroborated protein-level ANPEP expression in a subset of metaplastic cells within biopsy specimens from an independent cohort of patients with *Hp*- and AIG-induced metaplasia. Collectively, these findings reveal that *Hp* infection and AIG both promote the emergence of a cancer-associated incomplete IM that can be identified via ANPEP.

Materials and Methods

Murine Tissue Samples

C57BL/6 mice (The Jackson Laboratory, Bar Harbor, ME) were infected at age 6 to 8 weeks with $\sim 1\times10^8$ colony forming units of *Hp*, premouse Sydney strain 1.[20] Colony-forming units and pathology were confirmed in littermates 1 month after infection. Mice were euthanized between 6 and 13 months of infection. AIG was modeled in transgenic TxA23 mice, which express a T-cell receptor that recognizes a peptide found within the parietal cell-specific H^+/K^+- adenosinetriphosphatase presented on BALB/c MHCII.[21,22] To compare with C57BL/6-infected animals, BALB/c TxA23 animals were backcrossed to C57BL/6J animals expressing BALB/c MHC for 11 generations. TxA23 mice were humanely killed between age 3 and 7 months when metaplasia was prevalent. An equal mix of males and females were used across models. Mice were bred and maintained under specific pathogen-free conditions in our animal facility following Animal Research: Reporting of In Vivo

Experiments (ARRIVE) guidelines, approved by the Saint Louis University Department of Comparative Medicine (Association for Assessment and Accreditation of Laboratory Animal Care, 000656).

Human Study Approval

Healthy stomachs were obtained postmortem from Mid-America Transplant via a material transfer agreement. Gastric biopsy specimens from *Hp*-infected patients were obtained through a collaboration between Washington University in St. Louis School of Medicine and Universidad del Cauca under Institutional Review Board protocol 201901176. AIG biopsy specimens were obtained from adult patients who provided informed consent under Institutional Review Board protocol 202104160 (Supplementary Table 1). For the *Hp*-infected samples, an equal mix of sexes were used, but all AIG-derived samples were from women due to female predominance of disease.[23]

Histopathology

Stomachs from healthy, *Hp*-infected, and TxA23 mice were cut along the lesser curvature, rinsed, and fixed in 10% formalin (Thermo Fisher, Waltham, MA) for 24 hours. Stomachs were then cut, leaving strips to be embedded in paraffin, sectioned, and stained. Healthy human stomach sections were processed in a manner similar to mouse tissues. *Hp*-infected and AIG patient biopsy specimens were fixed in 4% paraformaldehyde for 2 hours at room temperature and embedded in paraffin for further processing. Light micrographs of tissue sections were taken on the DM6 Epifluorescence (Leica Microsystems, Wetzlar, Germany) at original magnification $\times$100. Three blinded, independent investigators scored tissues for pathology following established guidelines.[24]

Immunofluorescence

Methods to prepare and stain stomach tissue were adapted from previous work.[25] Briefly, paraffin-embedded 5-μm sections were deparaffinized with xylene, followed by isopropanol, and rehydrated with water. Antigen retrieval was achieved with pressurized incubation in 10 mmol/L sodium citrate (pH 6.0). Tissues were washed and incubated for 1 hour in blocking buffer (phosphate buffered saline, 1%; bovine serum albumin, 0.3%; and Triton X-100). Tissues were stained with primary antibodies overnight at 4°C, washed thrice, and stained with secondary antibodies for 1 hour at room temperature (Supplementary Table 2). Tissues were washed twice, stained with Hoechst (1:20,000; Invitrogen, Waltham, MA) for 5 minutes at room temperature, and mounted using ProLong Gold Antifade (Life Technologies, Carlsbad, CA). All images were taken on the Leica TCS SP8 confocal (Leica Microsystems) on original magnification $\times$200. Frequency of metaplastic glands was calculated as number of gastrokine 3-positive ($GKN3^+$) glands over total number of glands imaged.

Epithelial Single-Cell Isolation

Corpus tissues were obtained from 2 to 7 mice per group and 3 AIG patients. Tissues were rinsed and placed in a 50 mL conical with 10 mL gland digest buffer: Advanced Dulbecco's modified Eagle medium (Thermo Fisher), 20 mmol/L HEPES (Thermo Fisher), 0.2% bovine serum albumin (MilliporeSigma, Burlington, MA), 50 μg/mL gentamicin (MilliporeSigma), 1% penicillin/streptomycin (MilliporeSigma), and deoxyribonuclease I (100 U/mL; MilliporeSigma). Collagenase 1A (1 mg/mL; MilliporeSigma) was added to each tube before 37°C incubation with constant shaking for 20 to 45 minutes.

Samples were checked for the presence of gastric glands, rinsed, and spun down (50*g* for 10 minutes). Samples were resuspended in 1 mL/stomach prewarmed trypsin-EDTA (MilliporeSigma) and incubated for $\sim$25 minutes at 37°C, agitating every 5 to 10 minutes. Digestion was considered complete when single cells were observed. Cells were washed twice with Dulbecco's modified Eagle medium plus 10% fetal bovine serum. Cells were filtered twice, counted, and resuspended to a final cell concentration of $\sim$1000 cells/μL. Viability of each sample was confirmed to be $>$70% by trypan blue staining (Thermo Fisher).

Chromium Single-Cell Library Construction

Library construction of mouse tissues was performed at Saint Louis University, and construction of AIG human libraries was performed at Washington University in St. Louis Genome Technology Access Center. To generate libraries, the Chromium Controller (10X Genomics, Pleasanton, CA) was used following the manufacturer's protocols. Libraries were prepared using the Chromium Next GEM Single Cell 5′ Kit v2 (1000263, 10X Genomics). Each library was generated to have a maximum recovery of 10,000 cells. Polymerase chain reactions were conducted in the T100 Thermal Cycler (Bio-Rad, Hercules, CA). Final quality control was performed on the 2100 Bioanalyzer Instrument (Agilent, Santa Clara, CA), and libraries were sequenced on the NovaSeq 6000 (Illumina, San Diego, CA).

Human Data Download

Hp data sets from 10 *Hp*-positive gastric cancer patients were accessed via the Gene Expression Omnibus through accession number GSE150290 (Supplementary Methods).[26]

Data Processing and Statistical Analysis

Raw data were processed using cellranger-6. Conditional repeats were combined using cellranger aggr. Analysis was conducted using Seurat.[27] Each data set was filtered to exclude cells with low gene expression ($<$500 per cell), high gene counts (outliers), and high percentage mitochondrial transcript load ($>$25% per cell). Per species, data sets were merged, normalized, scaled, and dimensionally reduced. Layers were joined and clusters were generated using a resolution of 0.8 for mouse and 1.2 for human data sets. Cluster identities were established by attaining distinguishing genes per cluster and relating them to known profiles for gastric epithelial cells.

Signature scores were calculated using AddModuleScore. Scores were generated for each cell based on the overall average gene expression across signature transcripts. Signature scores were normalized by subtracting average expression of randomly selected control genes, resulting in a relative per-cell signature score. Signatures were extracted from the Molecular Signatures Database[28,29] or generated from known metaplasia- and cancer-associated transcripts (Supplementary Tables 3 and 4) or from cluster-defining transcripts within our data sets (Supplementary Tables 5 and 6). Epithelial cell label transfers were created by transferring cluster labels from the *Hp* tumor

biopsy specimens onto the metaplastic subclusters using the Satija Lab reference-mapping approach.[26]

Statistical analyses were performed in GraphPad Prism 9.3.0 (GraphPad Software) or Seurat. The significance of cluster-defining genes was calculated using Wilcoxon's rank sum test with Bonferroni's correction for multiple comparisons. *P* values of $<.05$ were considered significant.

Results

Pathologic Comparison of Helicobacter pylori and Autoimmune Gastritis Mouse Models of Disease

To compare the pathologic features of disease induced by *Hp* infection and AIG, we used 2 well-established mouse models. For *Hp* infection, C57BL/6 mice were infected with premouse Sydney strain 1, a wild-type human isolate that induces gastric metaplasia in mice.[20] To model AIG, the previously validated BALB/c TxA23 mouse model that develops histologic characteristics of human AIG was backcrossed to the C57BL/6 background for direct comparison to C57BL/6-infected mice.[21,22] By histopathologic evaluation of gastric corpus sections, models of *Hp* infection and AIG both induced moderate to severe inflammation, atrophy, mucous neck cell expansion, and mucosal hyperplasia (Figure 1*A*). Pathologic severity was less in *Hp* than in AIG, likely due to the multifocal inflammatory nature of *Hp* infection compared with the corpus-wide pathology seen with AIG (Figure 1*C*).[30] *Hp* mice showed mild inflammation

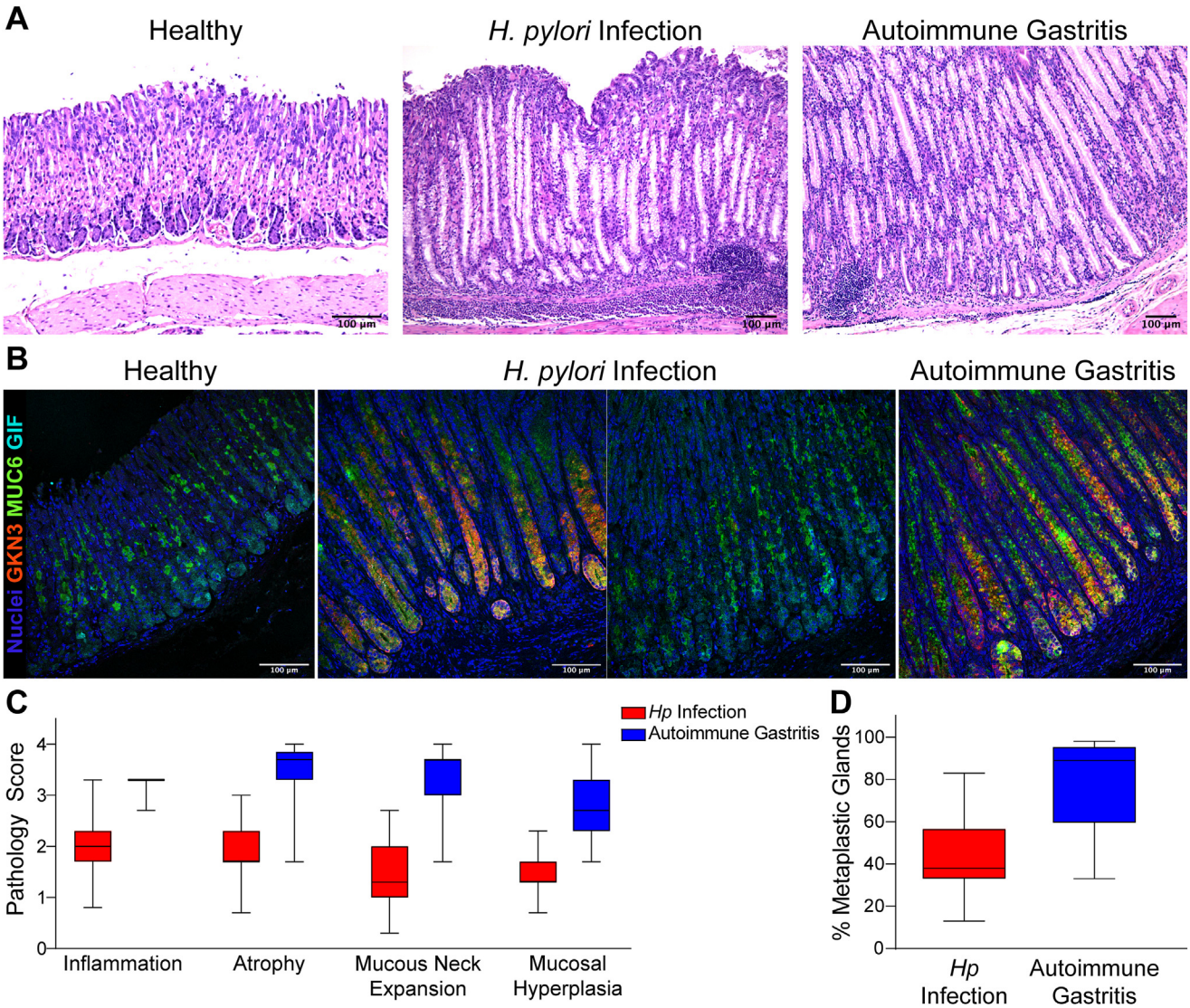

Figure 1. Similar gastric pathologies observed between models of *Hp* and AIG. (*A*) Representative hematoxylin and eosin images of corpora from a healthy (*left*), a 6-month *Hp*-infected (*center*), and a 6-month-old TxA23 (*right*) mouse. *Scale bars*: 100 μm. (*B*) Representative immunofluorescent images of corpora from a healthy (*left*), a 13-month *Hp*-infected diseased area (*center left*) and nondiseased area (*center right*), and a 6-month-old TxA23 (*right*) mouse. Tissue is stained with Hoechst (*blue*), GKN3 (*red*), MUC6 (*green*), and GIF (*cyan*). *Scale bars*: 100 μm. (*C*) Summary stomach pathology scores from 6- to 13-month-old *Hp*-infected (*red*, n = 15) and 4- to 6-month-old TxA23 (*blue*, n = 13) mice. Box-and-whisker plot: The *boxes* indicate the 25th percentile (*bottom border*), median (*center line*), and 75th percentile (*top border*), and the whiskers show the maximum and minimum ranges. (*D*) Quantification of GKN3$^+$ metaplastic glands between *Hp*-infected (n = 13) and AIG (n = 12) mice.

in the antrum, but neither model exhibited advanced antral pathology or neuroendocrine cell hyperplasia (Supplementary Figure 1). Nevertheless, in areas where disease was present, the histopathologic characteristics were similar between these 2 models.

To evaluate metaplasia in these 2 models, we performed immunofluorescent staining for mucin 6 (MUC6), gastric intrinsic factor (GIF), and GKN3. In healthy tissue, MUC6 and GIF displayed normal staining in healthy neck and chief cells, respectively (Figure 1*B*). Aberrant GKN3 staining and expanded MUC6 staining seen in both *Hp* and AIG identified metaplastic glands.[31] The proportion of glands containing metaplasia was ∼40% in *Hp*-infected mice compared with ∼80% in AIG mice (Figure 1*D*). Based on these findings, we conclude that in murine models of *Hp* infection and AIG, disease is nearly indistinguishable from a histopathologic perspective, with subtle differences in distribution.

Single-Cell Transcriptomic Comparison of Metaplasia Arising in Helicobacter pylori and Autoimmune Gastritis Models

To directly compare molecular phenotypes of metaplasia between diseases, single-cell RNA sequencing of cells from the corpora of *Hp*-infected mice and mice with AIG was conducted. The expected gastric cell types were identified in both *Hp* and AIG data sets, including metaplasia, parietal, neck, pit, chief, proliferating epithelial, enterochromaffin-like (ECL), and various immune cells (Figure 2*A*–*D*). We further identified metaplastic cells based on each cell's average expression across 17 gastric metaplasia-associated transcripts, such as trefoil factor 2 (*Tff2*), *Gkn3*, aquaporin 5 (*Aqp5*), and *Cd44* (Figure 2*B*–*D* and Supplementary Tables 3 and 4).[4,8,31,32] Separation of cells based on disease setting revealed similar patterns of metaplasia signature expression (Figure 2*C* and *D*). Metaplastic cells in the top 10th percentile of the gastric metaplasia signature were subset for unbiased repeat integration, normalization, and clustering. Most metaplastic cells were isolated from the metaplastic and neck cell clusters (Supplementary Table 7). Upon repeat clustering, 10 subclusters of gastric metaplasia were identified (Figure 2*E*).

Next, we evaluated the relative expression of gastric metaplasia-associated transcripts within each metaplastic subcluster (Figure 2*F*). All subclusters coexpressed *Tff2*, *Muc6*, *Gif*, and newly identified *Gkn3*, consistent with pyloric metaplasia.[31] These data demonstrate that the metaplastic cells originating from *Hp* and AIG models display similar transcriptional diversity.

Defining Metaplastic Subtypes That Arise Within Helicobacter pylori and Autoimmune Gastritis Models

Discovering transcriptionally diverse metaplastic cells through unsupervised clustering prompted us to focus on the features of metaplastic cells emerging within *Hp* infection and AIG. Among the 10 metaplastic subclusters, all were present across disease settings (Figure 3*A* and *B*), demonstrating that both models induce a similar repertoire of metaplastic subtypes.

To further define each metaplastic subcuster, we investigated cluster-specific gene expression. Five cluster-defining transcripts were mapped per metaplastic subcluster (Figure 3*C*). Several subtypes displayed transcript expression related to different gastric epithelial cells. Cluster 6 was enriched in foveolar cells defining *Gkn1* and *Gkn2*, and cluster 7 displayed a transcriptional profile akin to parietal cells, including *Atp4a* and *Atp4b*.[29] Other clusters were defined by transcripts associated with pyloric metaplasia, such as cluster 1 enriched in *Xist* and cluster 2 enriched in *Cd44*.[31,32] Differential expression of cluster-defining transcripts highlights the transcriptional diversity found within metaplastic cells.

Next, we performed signature analyses to gain insights into the phenotypes of the different metaplastic cells (Figure 3*D*–*G* and Supplementary Figure 2). We applied signatures obtained from the Molecular Signature Database, including for chief cells, intestinal stem cells, and ECL cells,[29] or that were generated from cluster-defining genes of our proliferative epithelial cell cluster (Supplementary Table 5). Scores were calculated to provide a normalized value based on expression across all genes within each signature. Cells in clusters 0 and 1 scored highest in the gastric chief cell signature (Figure 3*D*). Cells in clusters 1, 3, 4, and 7 scored highest for the intestinal stem cell signature. Cells in cluster 4, scored highest for the gastric proliferative cell signature. Finally, cells in clusters 5 and 8 scored highest for the ECL cell signature. Taken together, these findings underline that similar metaplastic phenotypes are induced between models of *Hp* and AIG.

Pathologic Comparison of Helicobacter pylori Infection and Autoimmune Gastritis in Human Disease

We next compared metaplasia induced in humans by analyzing biopsy specimens taken from patients with *Hp* infection and AIG. The pathologic features of disease observed in histopathology were similar between patients with *Hp* and AIG (Figure 4*A* and *B*). Pyloric and intestinal metaplasia was identified across settings (Figure 4*A*). Costaining with MUC6, TFF2, and CD44v9 identified pyloric metaplasia in the *Hp* and AIG biopsy specimens (Figure 4*B*). These results confirm that as in mouse models, metaplasia induced by *Hp* and AIG is difficult to distinguish in humans.

To compare metaplasia at cellular and molecular levels, single cells from corpus-derived biopsy specimens were analyzed via the same single-cell RNA sequencing pipeline applied to mouse models. Newly generated data sets included cells isolated from 3 AIG patients. All 3 patients were confirmed negative for *Hp*, and none had histologic evidence of gastric cancer (Supplementary Table 1). Additionally, 20 published data sets from tumor and tumor-adjacent corpus biopsy specimens from 10 *Hp*-positive patients with gastric cancer were downloaded (Figure 4*C*).[26] To compare metaplastic cells between *Hp* and AIG, cells

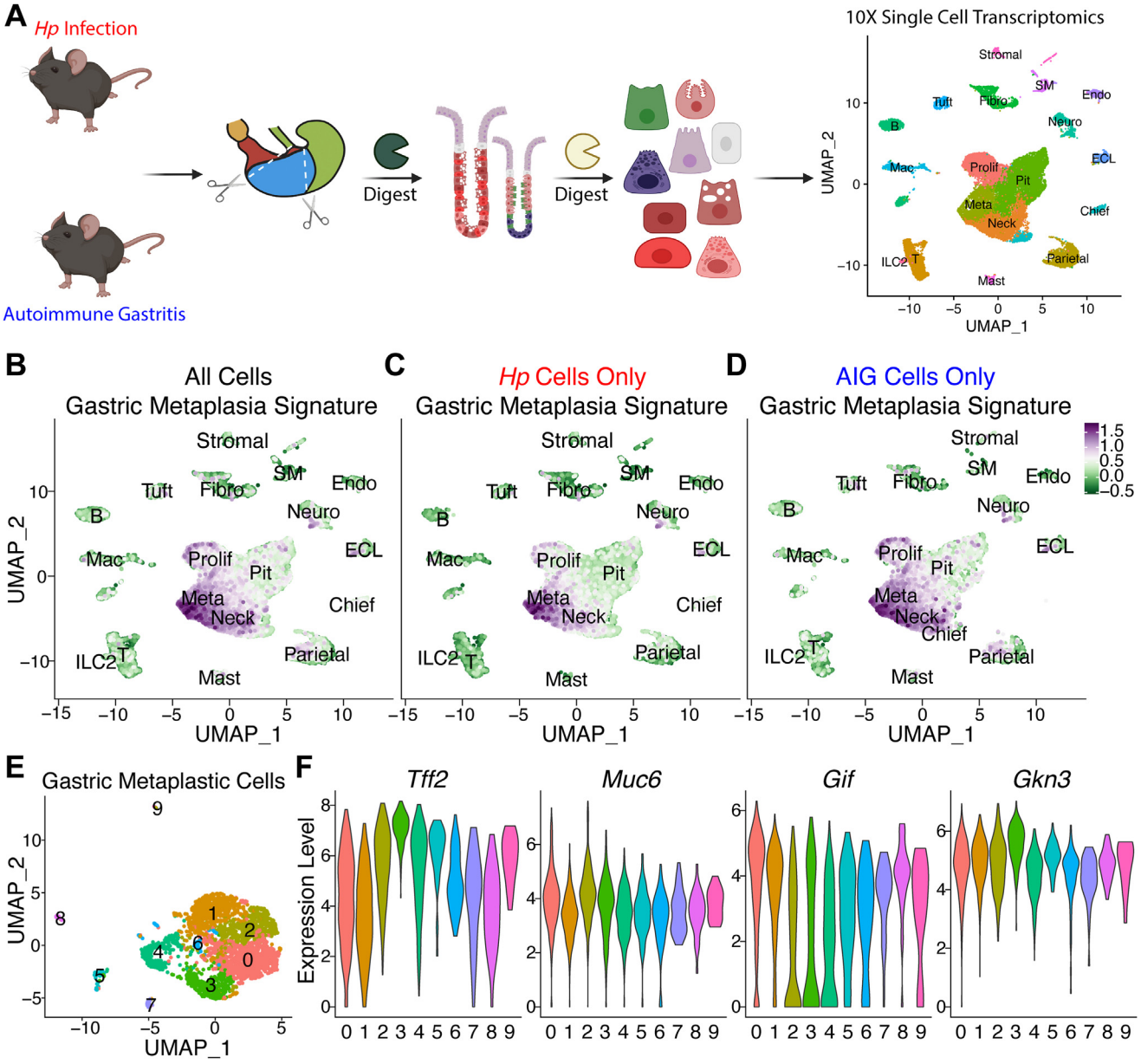

Figure 2. Metaplasia is transcriptionally similar across chronic inflammatory models. (*A*) Experimental design to run single-cell RNA sequencing on corpora of *Hp*-infected (n = 7, 16,000 cells analyzed) and AIG (n = 2, 12,000 cells analyzed) mice. (Stomach adapted from Willet SG, Mills JC. Stomach organ and cell lineage differentiation: from embryogenesis to adult homeostasis. Cell Mol Gastroenterol Hepatol 2016;2:546–559.) Feature UMAP visualizing epithelial cell clusters in (*B*) both, (*C*) *Hp* only, and (*D*) AIG only. UMAP is colored based on enrichment for the Gastric Metaplasia Signature Score. (*E*) UMAP of reclustered metaplastic cells colored by subcluster. (*F*) Violin plots measure expression levels of various metaplasia-associated transcripts for each subcluster.

from the tumor-adjacent specimens from *Hp*-infected patients were used, because most gastric cancers arise in a field of metaplasia.[4] All expected cell types were identified in both disease settings (Figure 4*D*). When a gastric metaplasia signature (Supplementary Table 3) was applied to these data, the highest-scoring cells from *Hp* and AIG settings mapped to the same clusters (Figure 4*D*). These data confirm that metaplastic cells in *Hp*-infected gastric cancer patients and patients with AIG are transcriptionally similar.

Single-Cell Transcriptomic Comparison of Metaplasia Arising in Helicobacter pylori and Autoimmune Gastritis Patients

Epithelial cells that scored in the top 10th percentile for the human metaplasia signature were isolated and subjected to unbiased reintegration and reclustering (Figure 5*A*). Most of the metaplasia signature-enriched cells were isolated from the metaplastic and neck cell clusters (Supplementary Table 8). This approach revealed that 12

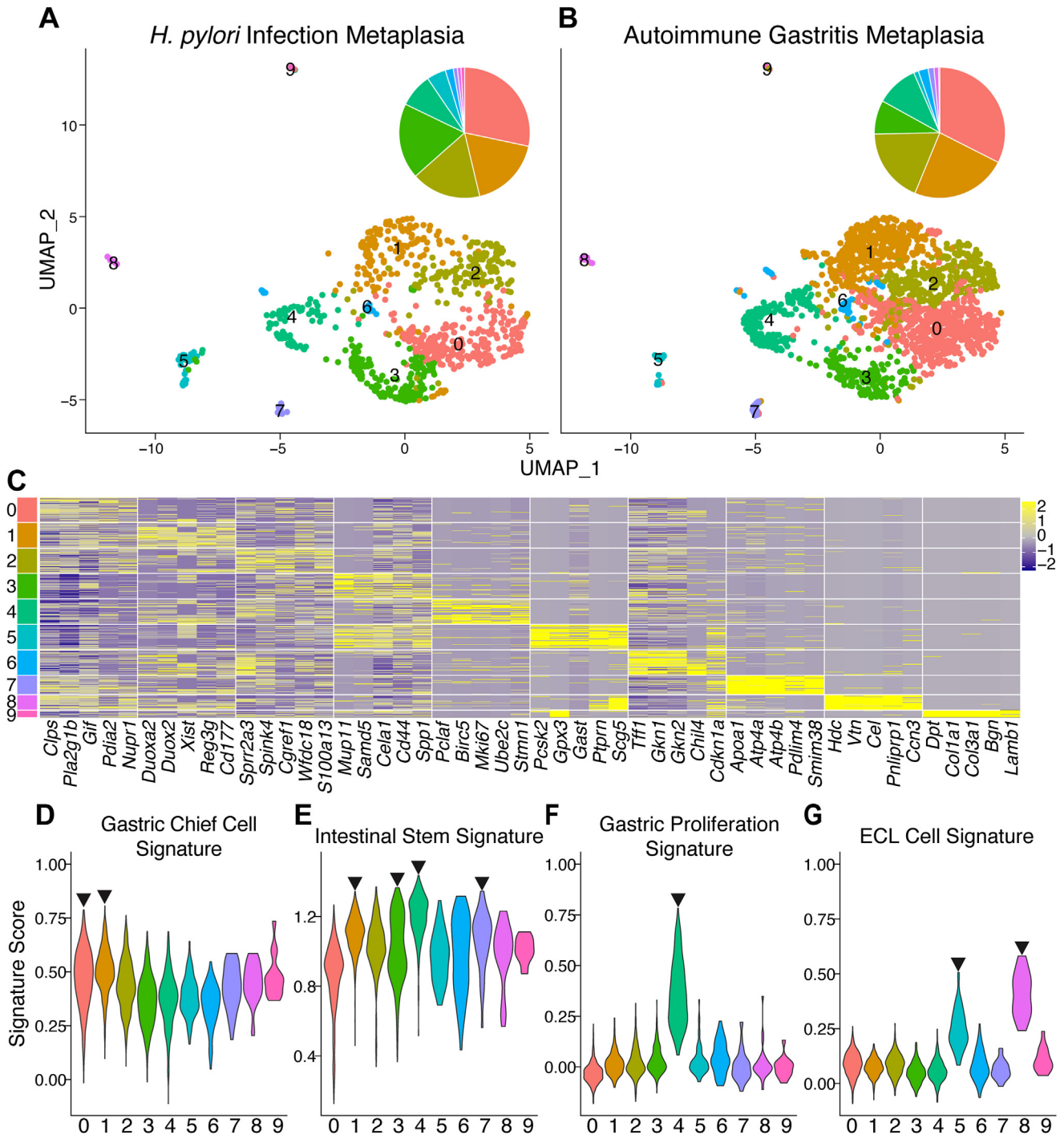

Figure 3. Common and diverse subtypes of metaplasia in mouse models of *Hp* and AIG. UMAP representing metaplastic cells found (*A*) only in *Hp* (900 cells analyzed) or (*B*) only in AIG (1900 cells analyzed). The pie charts show metaplasia subcluster frequencies. (*C*) Heat map of 5 cluster-defining transcripts for each metaplastic subcluster. (*D–G*) Violin plots visualize signature score for each metaplastic subcluster. The *black downward arrows* highlight highest scoring subcluster(s) for each signature. Plots are colored by subcluster identity.

metaplastic cell subtypes are present in biopsy specimens from *Hp*-infected and AIG patients.

When metaplastic subclusters were analyzed by disease, some metaplastic subtypes varied in frequency between *Hp* and AIG. For example, cells from subclusters 0 and 1 made up 60% of all metaplastic cells in the *Hp* biopsy specimens compared with only 20% in AIG specimens (Figure 5*B* and *C*). In fact, AIG biopsy specimens exhibited more diversity than *Hp*, containing all 12 metaplastic subtypes compared with 10 represented in *Hp*-infected biopsy specimens. Subclusters 10 and 11 were unique to AIG. These findings support that human gastric metaplasia is heterogeneous and

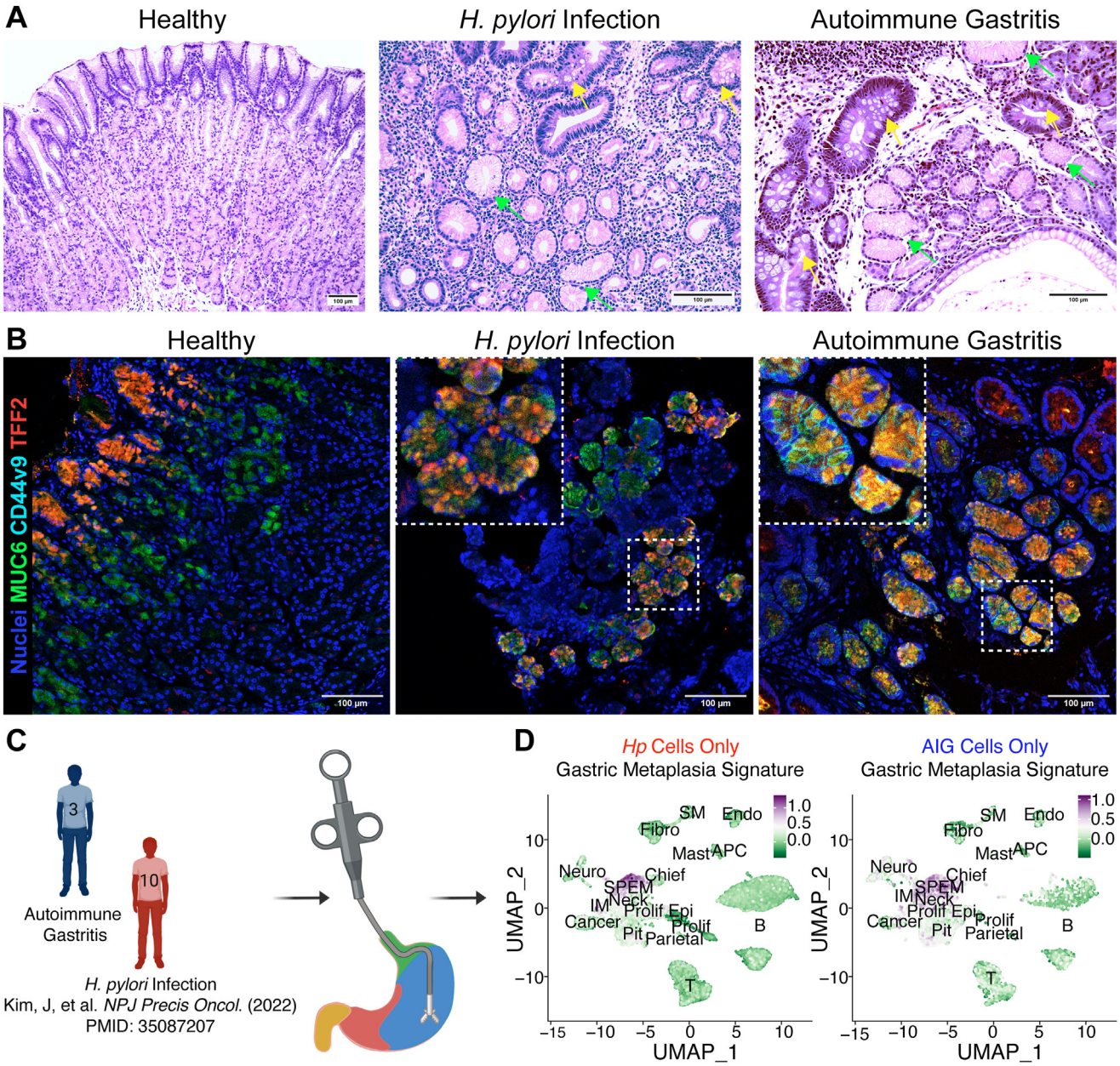

Figure 4. Similar gastric pathologies observed in *Hp* and AIG patient biopsy specimens. (*A*) Representative hematoxylin and eosin images of corpus from a healthy (*left*), a *Hp*-infected (*center*), and AIG (*right*) patient. *Arrows* highlight areas of intestinal (*yellow*) and pyloric (*green*) metaplasia. (*B*) Representative immunofluorescent images of corpus of a healthy (*left*), an *Hp*-infected (*center*), and an AIG (*right*) patient biopsy specimen. Tissue is stained with Hoechst (*blue*), MUC6 (*green*), CD44v9 (*cyan*), and TFF2 (*red*). (*C*) Experimental design for conducting single-cell RNA sequencing on *Hp*-infected (n = 10, 30,000 cells analyzed) and AIG (n = 3, 13,000 cells analyzed) patient biopsy specimens. (*D*) Feature UMAP visualizing epithelial cell clusters in *Hp* only (*left*) and AIG only (*right*). UMAP is colored based on enrichment for the Gastric Metaplasia Signature Score.

that inflammatory insult impacts the diversity of metaplastic cells. It is noteworthy that all metaplastic subtypes identified in *Hp*-infected patients with gastric cancer were also found in the AIG patients.

To validate that each subcluster was metaplastic, plots were generated to visualize expression of metaplasia-associated transcripts (Figure 5*D*). Most subclusters were highly enriched in expression of the spasmolytic polypeptide, *TFF2*, excluding subclusters 2 and 4. All subclusters except 9 expressed the neck cell-associated transcript *MUC6*. Cells in subclusters 8 and 9 expressed the highest levels of goblet cell transcript, *TFF3*, associated with IM. Tumor-associated calcium signal transducer 2 (*TACSTD2*), or TROP2, reported to be dysplasia-associated,[33] was up-regulated in several subclusters.

To further define each metaplastic subcluster, we highlighted the top 5 cluster-defining genes in a heat map (Figure 5*E*). Cluster-defining genes revealed that some

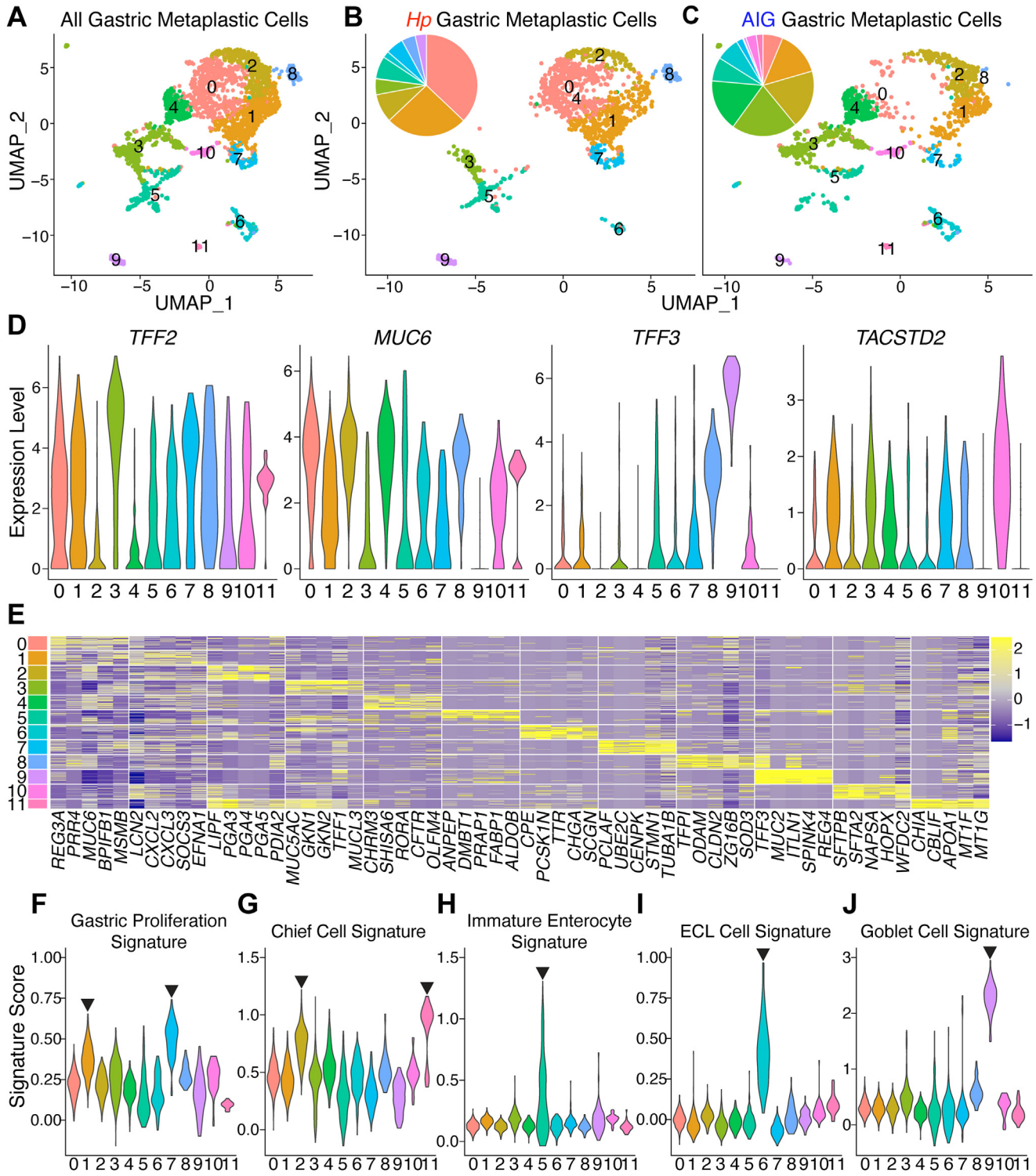

Figure 5. Heterogeneous gastric metaplastic cells identified across patient disease settings. (*A*) UMAP of reclustered metaplastic cells colored by subclusters. UMAP of metaplastic subclusters in (*B*) *Hp*-infected biopsy specimens (1400 cells analyzed) and (*C*) AIG biopsy specimens (1500 cells analyzed), colored by subcluster. The pie charts show subcluster frequencies. (*D*) Violin plots measuring expression levels of metaplasia- or dysplasia-associated transcripts for each metaplastic subcluster. (*E*) Heat map of 5 selected cluster-defining transcripts for each metaplastic subcluster. (*F–J*) Violin plots visualize signature score for each metaplastic subcluster. The *black downward arrows* highlight the highest scoring subcluster(s) for each signature. Plots are colored by subcluster identity.

subtypes expressed transcripts associated with gastric epithelial cells, such as cluster 2 resembling chief cells and cluster 3 resembling foveolar cells.[29] Other metaplastic clusters were enriched in pyloric metaplasia-associated transcripts, such as cluster 4 enriched in cystic fibrosis transmembrane conductance regulator (*CFTR*) and olfactomedin 4 (*OLFM4*)[34,35] and cluster 10 enriched in WAP four-disulfide core domain 2 (*WFDC2*).[36]

We then inferred characteristics of the metaplastic cells by performing signature analyses (Figure 5*F–J* and Supplementary Figure 3). As in the mouse analyses, human signatures were obtained from the Molecular Signature Database, including gene sets associated with chief cells, immature enterocytes, ECL cells, and goblet cells.[29] The gastric proliferation signature was generated from the proliferative epithelial cell cluster in our data set (Supplementary Table 6). Cells in subclusters 1 and 7 exhibited the highest scores for the gastric proliferative cell signature (Figure 5*F*). Cells in subcluster 2 and AIG-unique subcluster 11 scored highest for the chief cell signature (Figure 5*G*). Subcluster 5 scored highest in the immature enterocyte signature (Figure 5*H*). This finding, paired with the observed coexpression of *TFF2*, *MUC6*, *TFF3*, and *TACSTD2* in this cluster (Figure 5*D*), indicates that subcluster 5 is incomplete IM.[8,37] Metaplastic subcluster 6, present at double the frequency in AIG over *Hp* biopsy specimens, scored highest for the ECL cell signature (Figure 5*I*). Finally, cells in subcluster 9 scored highest for the goblet cell signature, identifying this cluster as complete IM (Figure 5*J*).[9] These findings taken together suggest that despite variability in metaplastic cell distributions between *Hp*-infected and AIG patients, the metaplastic subtypes associated with disease progression (proliferative metaplasia, complete IM, and incomplete IM) were identified in both settings.

Evaluating Relatedness to Cancer Across Metaplastic Subtypes

After identifying metaplastic subtypes, we designed an approach to determine transcriptional relatedness to cancer. A signature was generated using 20 gastric cancer-associated transcripts enriched in tumor over tumor-adjacent tissue data sets (Supplementary Table 3).[18,26,38,39] To validate that this signature could identify cancer cells, we first applied it to the *Hp*-infected tumor biopsy specimens instead of the tumor-adjacent specimens that were used to identify metaplastic subtypes. This signature successfully identified the cancer cluster in tumor specimens from the antrum and corpus, between which there was little transcriptional distinction (Figure 6*A* and Supplementary Figure 4).

Next, we applied this cancer signature to the newly defined metaplastic subtypes. This approach identified metaplastic subcluster 5 (incomplete IM) and to a lesser degree subcluster 9 (complete IM) as the metaplastic subtypes most enriched in the cancer signature (Figure 6*B* and *C*). As a confirmatory analysis, metaplastic subtypes were scrutinized based on transcriptional profile against epithelial cells identified in the *Hp*-infected tumor specimens. Label transfer of epithelial cell clusters was projected onto the metaplastic subtypes to predict which tumor-derived epithelial cell types were most transcriptionally associated with each metaplastic subcluster. Again, cluster 5 was the metaplastic subcluster most associated with cancer cells in both disease settings (Figure 6*D*). A proportion of cells in subclusters 0, 1, 3, 6, 7, 9, and 10 also mapped to cancer cells. Together, these findings identified subcluster 5, the incomplete IM subtype, as a cancer-related metaplastic cell arising in both *Hp* and AIG.

We next examined the cluster-defining transcripts for the cancer-related subcluster 5 to identify a potential cancer-associated biomarker. This analysis led to the identification of *ANPEP* as a subcluster 5-defining gene with low to undetectable expression in other metaplastic subtypes (Figures 5*F* and 6*E* and Supplementary Figure 5). We also confirmed that *ANPEP* was uniquely up-regulated within the cancer cluster from *Hp*-infected tumor biopsy specimens (Figure 6*F*). In summary, a metaplasia resembling incomplete IM was identified among the metaplastic cells found in patients with *Hp*- and AIG-induced metaplasia. This subcluster was the most transcriptionally related to gastric cancer and uniquely expressed high levels of *ANPEP.*

ANPEP/CD13 as a Biomarker for Cancer-Related Metaplasia in Helicobacter pylori and Autoimmune Gastritis Patients

Expression of *ANPEP* in the cancer-like, incomplete IM subtype led us to evaluate ANPEP protein expression in a separate cohort of patients with *Hp* or AIG (Figure 7). No detectable expression of intestinal metaplastic proteins TFF3 and MUC2 or ANPEP was found in healthy gastric tissue (Supplementary Figure 6). By hematoxylin and eosin staining, IM glands were identified in *Hp* and AIG biopsy specimens (Figure 7*A* and *B*). This was confirmed by positive staining for TFF3 and MUC2 (Figure 7*C* and *D*). In the same IM regions, ANPEP expression was observed (Figure 7*E* and *F*), confirming the expression of ANPEP in IM glands. Of the 5 *Hp* patients with IM screened, all had detectable ANPEP expression in a subset of IM glands (Supplementary Figure 7). Of the 6 AIG patients with IM tested, all had a subset of IM glands with detectable ANPEP expression. These data confirm the presence of ANPEP staining in a subset of metaplastic cells in several precancerous biopsy specimens from patients with *Hp*- and AIG-induced metaplasia. This suggests that ANPEP could serve as an early biomarker for patients at a heightened risk of cancer progression.

Discussion

Metaplasia serves a tissue healing role in settings of acute injury.[5,40] However, with long-standing injury, such as chronic inflammation, metaplasia persists and may transform into dysplasia.[41] But even in cases of chronic inflammation, cancer develops in only a small proportion of individuals.[6] There is a need to better characterize

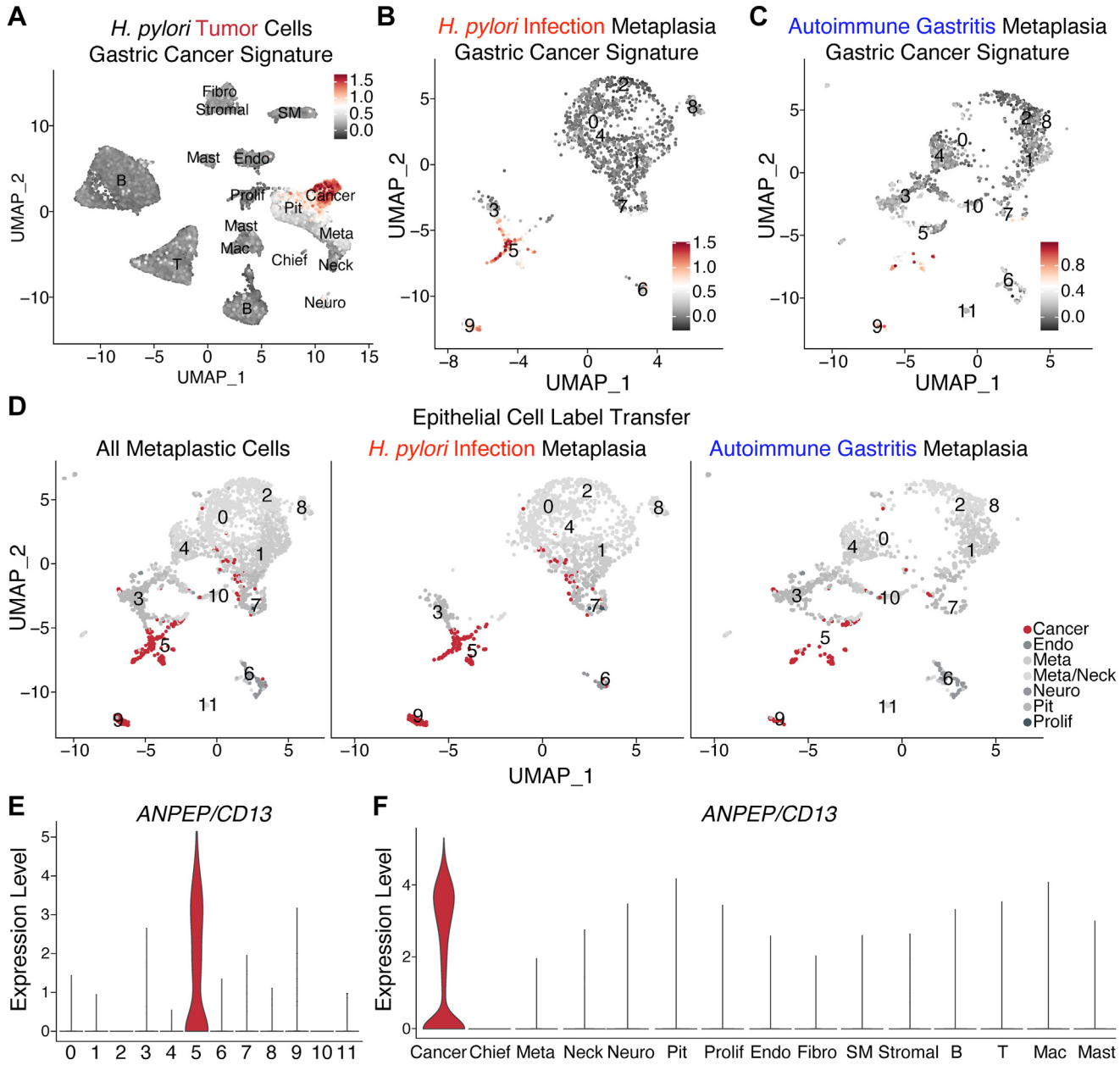

Figure 6. Cancer-related metaplastic cells present in patients with *Hp* and AIG. (*A*) Feature UMAP visualizing epithelial cell clusters in *Hp* tumor corpus biopsy specimens (n = 10, 30,000 cells analyzed). UMAP is colored based on enrichment for the Gastric Cancer Signature Score. (*B*) Gastric Cancer Signature feature UMAP for *Hp* metaplastic cells. (*C*) Gastric Cancer Signature feature UMAP for AIG metaplastic cells. (*D*) UMAP of gastric metaplastic subclusters in all settings (*left*), *Hp* only (*center*), or AIG only (*right*) labeled with epithelial cell clusters from *Hp* corpus tumor biopsy specimens. Violin plots demonstrate *ANPEP/CD13* transcript expression (*E*) across metaplastic subclusters and (*F*) across cell clusters in the *Hp* corpus tumor biopsy specimens.

metaplastic lineages at a high risk of cancer progression to improve prevention and therapeutic strategies.

Here we defined a transcriptionally diverse array of metaplastic cells present in distinct chronic inflammatory settings: *Hp* infection and AIG. Although variations were found in the frequency of certain metaplastic subtypes between diseases, most were shared. Of note, *Hp*, associated with a higher adenocarcinoma risk, did not induce unique metaplastic subtypes from AIG. Across mouse models and human disease, common metaplastic subtypes resembling chief and proliferative cells were confirmed, alongside subtypes exhibiting ECL and intestinal features.[7,34,42] We infer that the chief-like metaplastic cells are a chief-derived metaplastic cell through the process called paligenosis.[42,43] In humans, the ECL-like metaplasia was increased in frequency in AIG compared with *Hp*, suggesting a bias toward ECL transformation in the setting of autoimmunity, following the prominent association of neuroendocrine tumors in AIG.[14]

This analysis confirmed the presence of proliferative metaplastic cells.[44] In fact, the proliferative metaplastic cells

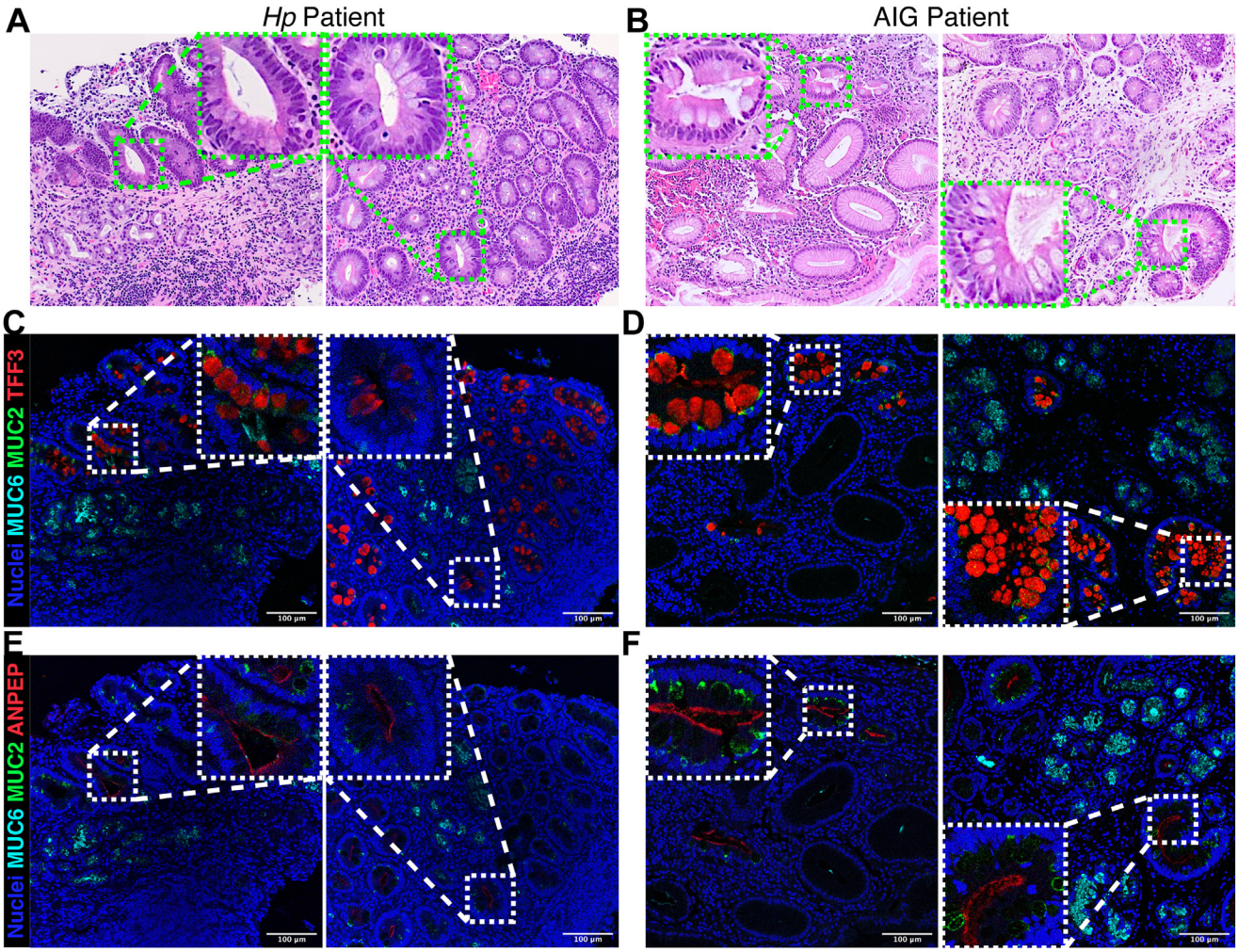

Figure 7. ANPEP/CD13 identifies cancer-related metaplastic cells in *Hp* and AIG metaplastic biopsy specimens. (*A* and *B*) Representative hematoxylin and eosin images of *Hp*-infected and AIG patient biopsy specimens highlight areas of metaplasia (magnification ×200). (*C–F*) Immunofluorescent images of *Hp*-infected (*left*) and AIG patient biopsy specimens (*right*). (*C* and *D*) Tissue is stained with Hoechst (*blue*), MUC6 (*cyan*), MUC2 (*green*), and TFF3 (*red*). (*E* and *F*) Tissue is stained with Hoechst (*blue*), MUC6 (*cyan*), MUC2 (*green*), and ANPEP (*red*). *Scale bars*: 100 μm. Sequential imaging of the same section was conducted between *A*, *C*, and *E* (*Hp*-infected) and *B*, *D*, and *F* (AIG).

in humans expressed dysplasia-associated *TACSTD2*, or TROP2,[33] and some were transcriptionally related to cancer. This suggests a cancer progression potential, although further investigation is warranted considering that this subtype was identified in mouse models that do not progress beyond metaplasia. We acknowledge the potential cancer risk of proliferative metaplastic cells, but here we focus on the more cancer-associated IM subtypes.

Mouse models of gastric metaplasia typically do not develop IM or cancer unless treated with carcinogens or genetically engineered,[45,46] but intestinalized SPEM cells have been previously identified.[34] These findings confirm the presence of metaplastic cells that express intestinal transcripts in *Hp* infection and AIG disease models, but no evidence of IM was identified by histopathology. The expected presence of IM was confirmed in human specimens, revealing distinct clusters for complete and incomplete IM. Our attention was particularly drawn toward the incomplete IM subtype due to its transcriptional resemblance to cancer cells and previous evidence suggesting a greater risk of adenocarcinoma compared with complete IM.[10] An incomplete IM metaplastic subtype was observed across both AIG and *Hp* infection settings, although prior studies have identified a lower prevalence of incomplete IM glands in AIG compared with *Hp*-induced gastritis.[47]

The question of whether AIG poses a similar risk of gastric cancer as *Hp* remains contentious, necessitating further investigation. Complicating matters, *Hp* infection may promote AIG, blurring the classification of each inflammatory driver's impact on cancer risk.[48] *Hp*-specific virulent factors, such as cytotoxin-associated gene A (CagA), are believed to play a pivotal role in driving cancerous lesions.[49] Nevertheless, it is noteworthy that cancer-related metaplastic cells developed in patients examined here from both disease settings. AIG appears to induce a broader spectrum of metaplastic phenotypes, some not observed in *Hp.*

We hypothesize that the expanded diversity of metaplasia in AIG as well as an increased prevalence of ECL-like metaplastic cells may bias it toward developing neuroendocrine tumors. Conversely, the more limited diversity of metaplastic phenotypes in *Hp* may predispose it toward adenocarcinoma progression. Nonetheless, the detectability of cancer-related metaplastic cells in all patients with IM suggests a risk for developing adenocarcinoma in both AIG and *Hp*. Despite the ongoing debate, emerging evidence hints at AIG's potential contribution to the rising rates of gastric adenocarcinoma among younger women.[13] These results support that AIG, like *Hp*, can promote the rise of cancer-associated metaplastic lesions and likely increases the risk of adenocarcinoma.

In our investigation of incomplete IM as a cancer-associated lesion, we identified *ANPEP* (aka *CD13*) as a subcluster-defining transcript. Aminopeptidase N (ANPEP) is so named for its enzymatic ability to cleave neutral amino acids from the N-terminus of peptides.[50] Although ANPEP is typically expressed by intestinal enterocytes, it has also been implicated in various tumor types, including gastric adenocarcinoma, although with conflicting results.[16,29,50] Recent studies have reported ANPEP as an associated transcript in high-risk IM and gastric cancer, particularly in non-*Hp* cases.[18]

Before this study, however, ANPEP had not been used to distinguish incomplete IM glands in precancerous patients with confirmed *Hp*- or AIG-induced metaplasia. Thus, our work suggests that ANPEP may be useful for specific detection of cancer-related incomplete IM in patients before cancer development, similar to what has been found with TROP2.[37] Although there are already guidelines to serially screen patients with identified incomplete IM, this currently requires combining multiple histologic methods and pathologic expertise and is not standardized across health systems.[51,52] Taken together, these findings highlight the potential for ANPEP to be a biomarker to detect advanced gastric metaplasia before cancer development in targeted populations.

Although our study compares the pathologies induced by *Hp* infection and AIG ultimately leading to the development of cancer-related metaplastic lesions, several limitations necessitate further investigation. First, mouse models and human disease differ in several ways: (1) These mouse models are useful for replicating early metaplastic lesions like pyloric metaplasia but rarely progress to IM and cancer, (2) *Hp*-infected mice have limited antral disease, unlike infected patients, and (3) AIG mice do not develop the neuroendocrine cell expansion observed in AIG patients. Also, these studies imply that metaplastic cells give rise to gastric adenocarcinoma, but it is important to note that other cells, such as isthmal stem cells, may also be cancer-deriving cells.[53] In fact, recent publications have focused on an intestinal stem cell-resembling IM as a higher-risk metaplastic cell type prevalent in antral disease over enterocyte-resembling IM, and further work comparing these lesions in the antrum and corpus will need to be conducted.[18,54]

The predictive potential of ANPEP as a biomarker for cancer-associated, incomplete IM requires further validation with larger sample sizes and prospective assessments. Additionally, ascertaining whether ANPEP expression extends across all subtypes of gastric adenocarcinoma or is limited to one remains crucial, because this cancer signature is biased toward the genomically stable type.[39,55] Furthermore, if ANPEP proves to be a biomarker of early cancer risk, exploring its detectability in the serum of gastric metaplasia and cancer patients could be useful, as was established in gallbladder carcinoma.[56] Moreover, considering that treatment with ANPEP inhibitors has shown therapeutic benefit in patients with drug-resistant gastric cancer, further investigation into ANPEP as a target for therapeutic intervention is needed.[57]

Given that recent studies have found conserved features of metaplasia between the stomach, pancreas, and esophagus[58–60] and that ANPEP has been found to be enriched in other cancer types,[19,50] it will be important to establish whether ANPEP can be used to identify cancer-associated lesions in other gastrointestinal organs. Establishing the utility of ANPEP as an early biomarker across different cancer types will be imperative.

Conclusion

This study underscores the significance of comparing the features of metaplasia induced by *Hp* infection and AIG, revealing that both conditions induce cancer-associated metaplasia. As such, it emphasizes the importance of closely monitoring patients with either disease for early biomarkers, such as ANPEP/CD13, to mitigate adenocarcinoma risk and improve patient outcomes.

Supplementary Material

Note: To access the supplementary material accompanying this article, visit the online version of *Gastroenterology* at www.gastrojournal.org, and at https://dx.doi.org/10.1053/j.gastro.2024.08.032.

References

1. Sung H, Ferlay J, Siegel R, et al. Global cancer statistics 2020: GLOBOCAN estimates of incidence and mortality worldwide for 36 cancers in 185 countries. CA Cancer J Clin 2021;71:209–249.
2. Matsuzaka M, Tanaka R, Sasaki Y. High mortality rate of stomach cancer caused not by high incidence but delays in diagnosis in Aomori Prefecture, Japan. Asian Pac J Cancer Prev 2016;17:4723–4727.
3. Correa P, Piazuelo MB. The gastric precancerous cascade. J Dig Dis 2012;13:2–9.
4. Schmidt PH, Lee JR, Joshi V, et al. Identification of a metaplastic cell lineage associated with human gastric adenocarcinoma. Lab Invest 1999;79:639–646.
5. Engevik AC, Feng R, Choi E, et al. The development of spasmolytic polypeptide/TFF2-expressing metaplasia (SPEM) during gastric repair is absent in the aged stomach. Cell Mol Gastroenterol Hepatol 2016;2:605–624.

6. Song H, Ekheden IG, Zheng Z, et al. Incidence of gastric cancer among patients with gastric precancerous lesions: observational cohort study in a low risk Western population. BMJ 2015;351:h3867.
7. Goldenring JR, Mills JC. Cellular Plasticity, Reprogramming, and regeneration: metaplasia in the stomach and beyond. Gastroenterology 2022;162:415–430.
8. **Lee SH, Jang B, Min J**, et al. Up-regulation of aquaporin 5 defines spasmolytic polypeptide-expressing metaplasia and progression to incomplete intestinal metaplasia. Cell Mol Gastroenterol Hepatol 2021;13:199–217.
9. Correa P, Piazuelo MB, Wilson KT. Pathology of gastric intestinal metaplasia: clinical implications. Am J Gastroenterol 2010;105:493–498.
10. Piazuelo MB, Bravo LE, Mera RM, et al. The Colombian Chemoprevention Trial: 20-year follow-up of a cohort of patients with gastric precancerous lesions. Gastroenterology 2021;160:1106–1117.e3.
11. Plummer M, Franceschi S, Vignat J, et al. Global burden of gastric cancer attributable to *Helicobacter pylori*. Int J Cancer 2015;136:487–490.
12. Shah SC, Halvorson AE, Lee D, et al. *Helicobacter pylori* burden in the United States according to individual demographics and geography: a nationwide analysis of the Veterans Healthcare System. Clin Gastroenterol Hepatol 2024;22:42–50.e26.
13. Oh J, Abboud Y, Burch M, et al. Rising incidence of noncardia gastric cancer among young women in the United States, 2000-2018: a time-trend analysis using the USCS Database. Cancers (Basel) 2023;15:2283.
14. Rugge M, Bricca L, Guzzinati S, et al. Autoimmune gastritis: long-term natural history in naïve *Helicobacter pylori*–negative patients. Gut 2023;72:30–38.
15. **Chen C, Yang Y**, Li P, et al. Incidence of gastric neoplasms arising from autoimmune metaplastic atrophic gastritis: a systematic review and case reports. J Clin Med 2023;12:1062.
16. Kawamura J, Shimada Y, Kitaichi H, et al. Clinicopathological significance of aminopeptidase N/CD13 expression in human gastric carcinoma. Hepatogastroenterology 2007;54:36–40.
17. Uhlén M, Fagerberg L, Hallström BM, et al. Proteomics. Tissue-based map of the human proteome. Science 2015;347:1260419.
18. **Huang RJ, Wichmann IA**, Su A, et al. A spatially mapped gene expression signature for intestinal stem-like cells identifies high-risk precursors of gastric cancer. bioRxiv [Preprint] 2023.09.20.558462.
19. The Human Protein Atlas. Expression of ANPEP in cancer. Available at: https://www.proteinatlas.org/ENSG00000166825-ANPEP/pathology/stomach+cancer#ihc. Accessed April 23, 2024.
20. Dyer V, Brüggemann H, Sörensen M, et al. Genomic features of the *Helicobacter pylori* strain PMSS1 and its virulence attributes as deduced from its in vivo colonisation patterns. Mol Microbiol 2018;110:761–776.
21. McHugh RS, Shevach EM, Margulies DH, et al. A T cell receptor transgenic model of severe, spontaneous organ-specific autoimmunity. Eur J Immunol 2001; 31:2094–2103.
22. Nguyen TL, Khurana SS, Bellone CJ, et al. Autoimmune gastritis mediated by CD4+ T cells promotes the development of gastric cancer. Cancer Res 2013; 73:2117–2126.
23. Miceli E, Vanoli A, Lenti MV, et al. Natural history of autoimmune atrophic gastritis: a prospective, single centre, long-term experience. Aliment Pharmacol Ther 2019;50:1172–1180.
24. Rogers AB. Histologic scoring of gastritis and gastric cancer in mouse models. Methods Mol Biol 2012; 921:189–203.
25. Noto CN, Hoft SG, Bockerstett KA, et al. IL-13 acts directly on gastric epithelial cells to promote metaplasia development during chronic gastritis. Cell Mol Gastroenterol Hepatol 2021;13:623–642.
26. Kim J, Park C, Kim KH, et al. Single-cell analysis of gastric pre-cancerous and cancer lesions reveals cell lineage diversity and intratumoral heterogeneity. NPJ Precis Oncol 2022;6:9.
27. Hao Y, Stuart T, Kowalski MH, et al. Dictionary learning for integrative, multimodal and scalable single-cell analysis. Nat Biotechnol 2024;42:293–304.
28. Subramanian A, Tamayo P, Mootha VK, et al. Gene set enrichment analysis: a knowledge-based approach for interpreting genome-wide expression profiles. Proc Natl Acad Sci U S A 2005;102:15545–15550.
29. Busslinger GA, Weusten BLA, Bogte A, et al. Human gastrointestinal epithelia of the esophagus, stomach, and duodenum resolved at single-cell resolution. Cell Rep 2021;34:108819.
30. Lahner E, Zagari RM, Zullo A, et al. Chronic atrophic gastritis: Natural history, diagnosis and therapeutic management. A position paper by the Italian Society of Hospital Gastroenterologists and Digestive Endoscopists [AIGO], the Italian Society of Digestive Endoscopy [SIED], the Italian Society of Gastroenterology [SIGE], and the Italian Society of Internal Medicine [SIMI]. Dig Liver Dis 2019;51:1621–1632.
31. **Bockerstett KA, Lewis SA**, Noto CN, et al. Single-cell transcriptional analyses identify lineage-specific epithelial responses to inflammation and metaplastic development in the gastric corpus. Gastroenterology 2020; 159:2116–2129.e4.
32. Wada T, Ishimoto T, Seishima R, et al. Functional role of CD44v-xCT system in the development of spasmolytic polypeptide-expressing metaplasia. Cancer Sci 2013; 104:1323–1329.
33. Riera KM, Jang B, Min J, et al. Trop2 is upregulated in the transition to dysplasia in the metaplastic gastric mucosa. J Pathol 2020;251:336–347.
34. Weis VG, Sousa JF, LaFleur BJ, et al. Heterogeneity in mouse spasmolytic polypeptide-expressing metaplasia lineages identifies markers of metaplastic progression. Gut 2013;62:1270–1279.
35. Lee HJ, Nam KT, Park HS, et al. Gene expression profiling of metaplastic lineages identifies CDH17 as a prognostic marker in early stage gastric cancer. Gastroenterology 2010;139:213–225.e3.
36. Nozaki K, Ogawa M, Williams JA, et al. A molecular signature of gastric metaplasia arising in response to

acute parietal cell loss. Gastroenterology 2008; 134:511–522.
37. Jang B, Lee SH, Dovirak I, et al. CEACAM5 and TROP2 define metaplastic and dysplastic transitions in human antral gastric precancerous lesions and tumors. Gastric Cancer 2024;27:263–274.
38. **Lee SH, Contreras Panta EW, Gibbs D**, et al. Apposition of fibroblasts with metaplastic gastric cells promotes dysplastic transition. Gastroenterology 2023;165:374–390.
39. **Li B, Zhang F**, Niu Q, et al. A molecular classification of gastric cancer associated with distinct clinical outcomes and validated by an XGBoost-based prediction model. Mol Ther Nucleic Acids 2023;31:224–240.
40. Goldenring JR. Pyloric metaplasia, pseudopyloric metaplasia, ulcer-associated cell lineage and spasmolytic polypeptide-expressing metaplasia: reparative lineages in the gastrointestinal mucosa. J Pathol 2018;245:132–137.
41. Graham DY, Rugge M, Genta RM. Diagnosis: gastric intestinal metaplasia—what to do next? Curr Opin Gastroenterol 2019;35:535–543.
42. Nam KT, Lee HJ, Sousa JF, et al. Mature chief cells are cryptic progenitors for metaplasia in the stomach. Gastroenterology 2010;139:2028–2037.e9.
43. Willet SG, Lewis MA, Miao ZF, et al. Regenerative proliferation of differentiated cells by mTORC1-dependent paligenosis. EMBO J 2018;37:e98311.
44. Jeong S, Choi E, Petersen CP, et al. Distinct metaplastic and inflammatory phenotypes in autoimmune and adenocarcinoma-associated chronic atrophic gastritis. United European Gastroenterol J 2017;5:37–44.
45. Petersen CP, Mills JC, Goldenring JR. Murine models of gastric corpus preneoplasia. Cell Mol Gastroenterol Hepatol 2017;3:11–26.
46. Won Y, Choi E. Mouse models of Kras activation in gastric cancer. Exp Mol Med 2022;54:1793–1798.
47. Genta RM, Turner KO, Robiou C, et al. Incomplete intestinal metaplasia is rare in autoimmune gastritis. Dig Dis 2023;41:369–376.
48. Hoft SG, Noto CN, DiPaolo RJ. Two distinct etiologies of gastric cancer: infection and autoimmunity. Front Cell Dev Biol 2021;9:752346.
49. Freire de Melo F, Marques HS, Rocha Pinheiro SL, et al. Influence of *Helicobacter pylori* oncoprotein CagA in gastric cancer: a critical-reflective analysis. World J Clin Oncol 2022;13:866–879.
50. Lendeckel U, Karimi F, Al Abdulla R, et al. The role of the ectopeptidase APN/CD13 in Cancer. Biomedicines 2023;11:724.
51. Gupta S, Li D, El Serag HB, et al. AGA Clinical Practice Guidelines on Management of Gastric Intestinal Metaplasia. Gastroenterology 2020;158:693–702.
52. Tjandra D, Busuttil RA, Boussioutas A. Gastric intestinal metaplasia: challenges and the opportunity for precision prevention. Cancers (Basel) 2023;15:3913.
53. Hata M, Hayakawa Y, Koike K. Gastric stem cell and cellular origin of cancer. Biomedicines 2018;6:100.
54. Huang KK, Ma H, Chong RHH, et al. Spatiotemporal genomic profiling of intestinal metaplasia reveals clonal dynamics of gastric cancer progression. Cancer Cell 2023;41:2019–2037.e8.
55. Cancer Genome Atlas Research Network. Comprehensive molecular characterization of gastric adenocarcinoma. Nature 2014;513:202–209.
56. Priya R, Jain V, Akhtar J, et al. Plasma-derived candidate biomarkers for detection of gallbladder carcinoma. Sci Rep 2021;11:23554.
57. Niimoto M, Hattori T. Prospective randomized controlled study on bestatin in resectable gastric cancer. Biomed Pharmacother 1991;45:121–124.
58. Ma Z, Lytle NK, Chen B, et al. Single-cell transcriptomics reveals a conserved metaplasia program in pancreatic injury. Gastroenterology 2022;162:604–620.e20.
59. **Zeng Y, Li QK**, Roy S, et al. Shared features of metaplasia and the development of adenocarcinoma in the stomach and esophagus. Front Cell Dev Biol 2023;11:1151790.
60. Nowicki-Osuch K, Zhuang L, Cheung TS, et al. Single-cell RNA sequencing unifies developmental programs of esophageal and gastric intestinal metaplasia. Cancer Discov 2023;13:1346–1363.

Received April 23, 2024. Accepted August 28, 2024.

Correspondence
Address correspondence to: Richard J. DiPaolo, PhD, Department of Molecular Microbiology and Immunology, Saint Louis University School of Medicine, 1100 South Grand Boulevard, DRC707, St. Louis, Missouri 63104. e-mail: richard.dipaolo@health.slu.edu.

Acknowledgments
The authors thank Dr Richard M. Peek Jr (Vanderbilt University Medical Center, Nashville, TN) for generously providing the *Helicobacter pylori* strain premouse Sydney strain 1, thank Dr Jason C. Mills (Baylor College of Medicine, Houston, TX) and Dr David H. Alpers (Washington University in St. Louis School of Medicine, St. Louis, MO) for generously providing the gastrokine 3 and gastric intrinsic factor antibodies, respectively, and thank Caroline Murphy at the Saint Louis University Advanced Spatial Biology and Research Histology Facility for supporting the histopathology results provided in this report. The authors also acknowledge Biorender.com for facilitating the creation of animated figures.

CRediT Authorship Contributions
Stella Garden Hoft, BA (Conceptualization: Supporting; Data curation: Lead; Formal analysis: Lead; Funding acquisition: Supporting; Investigation: Supporting; Methodology: Equal; Validation: Lead; Visualization: Lead; Writing – original draft: Lead; Writing – review & editing: Lead)
Michelle Brennan, PhD (Formal analysis: Supporting; Writing – review & editing: Supporting)
Javier A. Carrero, PhD (Writing – review & editing: Supporting)
Nicholas M. Jackson, BS (Conceptualization: Supporting; Data curation: Supporting)
Challen A. Pretorius, MS (Writing – review & editing: Supporting)
Tarin M. Bigley, MD, PhD (Data curation: Equal; Funding acquisition: Supporting; Resources: Supporting; Writing – review & editing: Supporting)
José B. Sáenz, MD, PhD (Conceptualization: Supporting; Data curation: Supporting; Funding acquisition: Supporting; Resources: Supporting; Writing – review & editing: Supporting)
Richard J. DiPaolo, PhD (Conceptualization: Lead; Funding acquisition: Lead; Investigation: Lead; Methodology: Equal; Resources: Lead; Supervision: Lead; Writing – review & editing: Supporting)

Conflicts of interest
The authors disclose no conflicts.

Funding
This work was supported by the National Institute of Diabetes and Digestive and Kidney Diseases (NIDDK) under 2R56DK110406-06A1, R01DK134531, F30DK134124, 1K08DK122116, and R03DK133243. Funding for Tarin Bigley for this project was provided by the Children's Discovery Institute of Washington University (MI-FR-2022-990) and St. Louis Children's Hospital Scholar's Award.

Data Availability
The raw and processed single cell RNA sequenced libraries generated in these studies are available on the Gene Expression Omnibus under accession number GSE271866, and the R code to generate figures has been published on our GitHub repository (github.com/hoftsg/Hoft_et_al_2024.git).